
Article:
Jovanovic, V.D., Harrison, P., Ikonic, Z. et al. (2004) Physical model of quantum-well infrared photodetectors. Journal of Applied Physics, 96 (10). pp. 269-272. ISSN: 1089-7550

https://doi.org/10.1063/1.1756691

A physical model of quantum well infrared photodetectors (QWIPs)

V. D. Jovanović*, P. Harrison, Z. Ikonić, D. Indjin

School of Electronic and Electrical Engineering,

University of Leeds, Leeds LS2 9JT, United Kingdom

Abstract

A fully quantum mechanical model for electron transport in quantum well infrared photodetectors is presented, based on a self-consistent solution of the coupled rate equations. The important macroscopic parameters like current density, responsivity and capture probability can be estimated directly from this first principles calculation. The applicability of the model was tested by comparison with experimental measurements from a GaAs/AlGaAs device, and good agreement was found. The model is general and can be applied to any other material system or QWIP design.

* Electronic mail: eenvj@leeds.ac.uk

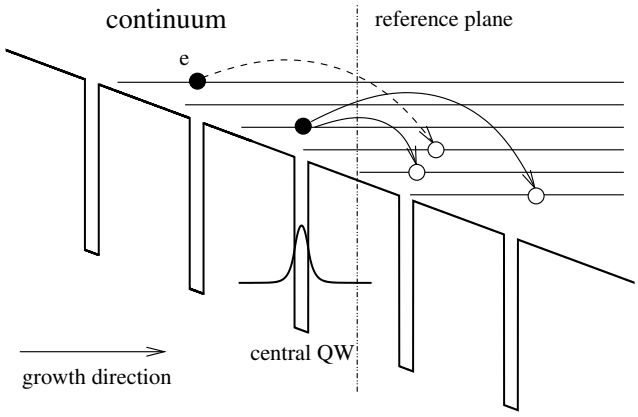

FIG. 1: Schematic diagram of the conduction band profile and electron scattering transport in QWIPs.

In the past decade quantum well infrared photodetectors (QWIPs) have reached a technological maturity as devices offering excellent performance in the mid- ($3-5\mu$m) and long-wavelength ($8-14\mu$m) infrared spectral range [1]. A large number of papers have been published, covering different aspects of QWIP design, modelling and characterization, delivering tunable, broadband and multicolor operation [2–8]. Moreover, large, highly uniform QWIP focal plane arrays have been reported with a wide range of possible applications [9, 10]. However, despite the extensive amount of experimental and theoretical efforts, not much work has been done on a microscopic quantum description of the processes that govern both vertical and parallel electron transport in periodic quantum structures, involving bound-bound and bound-continuum intersubband transitions [6, 11–13]. In order to ensure further improvement of the QWIP technology, primarily by using novel structures and material systems, a thorough understanding of fundamental physical procesess in QWIPs, as well as a first principles simulation tool are neccesary.

In this paper, two main topics are addressed: (i) development of a fully quantum mechanical model for the simulation of electron transport in QWIPs yielding physical observables like dark current density, responsivity, and capture probability, (ii) verification of the model by comparison with experimental data for GaAs/AlGaAs QWIPs detecting around 8.5μm.

Consider a multiple quantum well (MQW) structure with a large number of periods in an externally applied electric field. The energy spectrum is formally continuous, but to a very good approximation can be considered as consisting of quasi-discrete states (resonances). Based on the wavefunction localization properties, these states can be associated to different single QWs (i.e. periods) of the MQW, so that each period has an indentical set of N states in the energy range of interest. Electron scattering occurs between states within the same period, and between states

associated to different periods, the latter clearly becoming less effective for more distant periods because of reduced wavefunction overlap. Assuming an identical electron distribution in each period, one may consider some 'central' period and take its P nearest neighbours on either side, and write the scattering rate equations in the steady-state :

$$\begin{aligned}\frac{dn_i}{dt} = 0 = &\sum_{j=1,j\neq i}^{N} n_j W_{j,i} - n_i \sum_{j=1,j\neq i}^{N} W_{i,j} \\ &+ \sum_{k=1}^{P}\sum_{j=1,j\neq i}^{N} \left\{ n_j \left[W_{j,i+kN} + W_{j+kN,i} \right] \right. \\ &\left. - n_i \left[W_{i+kN,j} + W_{i,j+kN} \right] \right\} + \xi \times C(\Phi, n_1, n_2, ..) \end{aligned} \tag{1}$$

where $i+kN$ is the ith state of the kth neighbouring period, $W_{i,j}$ is the total scattering rate from state i into state j, n_i is the electron concentration of the ith state and ξ is equal to 1 for light and 0 for dark conditions. The first two sums in Eq.1 are due to intra-period, and the third due to inter-period scattering, while the term $C(.)$ describes the non-scattering contribution to electron transition rates. This is the rate at which electrons transfer between pairs of states due to intersubband absorption of incident radiation. After solving for electron densities n_i, macroscopic parameters of the system like current density, capture probability, responsivity, and drift velocity can be estimated.

The current density can be calculated by subtracting the current density component due to electrons scattering into the next periods of the MQW structure from the component due to electrons scattering back, as is usually done in quantum cascade laser simulations [14]. If we put a reference plane somewhere in the right barrier of the central QW, the current density flowing throught that cross section can be written as (Fig. 1):

$$J = \sum_{k=1}^{P}\sum_{i=1}^{N}\sum_{j=1}^{N} k \cdot n_i \left(W_{i,j+kN} - W_{i+kN,j} \right) \tag{2}$$

This expression defines both the dark and light current dependence on the value of the parameter ξ. The factor k in the summation, effective for non-nearest-neighbour scattering, comes from scatterings from any QW left of the centre well into any QW right of it, or vice versa (i.e. skipping the central well, but going through the reference plane). This current density component is presented with the dashed arrow on Fig. 1. With the current density known, the responsivity can be expressed as

$$R = \frac{J(\xi = 1) - J(\xi = 0)}{(hc/\lambda)\Phi} \tag{3}$$

where λ is the detection wavelength and Φ the total optical flux.

Another important parameter is the capture probability in standard drift-diffusion simulations usually taken as an empirical parameter representing quantum mechanical behavior of the QWs. Here we define the capture probability as the ratio of the electron current density component due to scattering from continuum states into quasi-discrete states of the QWs and the current component in continuum [12]. If the number of quasi-discrete states within the central QW is N_b then the capture probability can be expressed as

$$p_c = \frac{\sum_{k=1}^{P} J_k}{J} = \frac{\sum_{k=1}^{P}\sum_{i=N_b}^{N}\sum_{j=1}^{N_b} n_i W_{i,j}}{J} \tag{4}$$

A very important issue is the choice of wavefunctions assigned to a certain period, as the continuum states are not confined within a defined area and a wrong choice can lead to duplicated states and false estimate of the carrier dynamics. We define states belonging to the considered period as those having a better overlap integral with the ground state of that period than with the ground states of the neighbouring periods. For this purpose we define the overlap integral as $O_{ij} = \int |\psi_i(z)|^2 |\psi_j(z)|^2 dz$.

In order to reduce the number of scattering rate processes necessary to calculate the electron distribution and the corresponding current density (note that the number of total scattering rate processes is equal to $N^2(2P+1)-N$), we introduce the 'tight-binding' approximation assuming that only a few closest neighbors interact, and set $P = 2$. The choice of quantum scattering mechanisms depends on the material and doping density, as well as the detection wavelength. The k-space scattering rate averaging assumed Fermi-Dirac distribution within each subband with a unique electron temperature.

The optical perturbation constant, in the steady state conditions, is modelled assuming linear dependence on optical flux as:

$$C(\Phi, n_i, n_f) = A_{if}(n_i, n_f) \times \Phi \tag{5}$$

where A_{if} is fractional optical apsorption on the $i \rightarrow f$ transition calculated as in Ref. [15]. In general, A_{if} is a function of subband sheet electron densities. However, it is valid to assume that the electron concentration in the ground state is much larger than in the continuum states (note that this is justified under low illumination conditions, a reasonable assumption for most QWIP structures), which sets A_{if} as a constant in the self-consistent process. Furthermore, the diffraction grating influences the optical constant to some extent, and can in principle be included in the model, but this is out of the scope of this work.

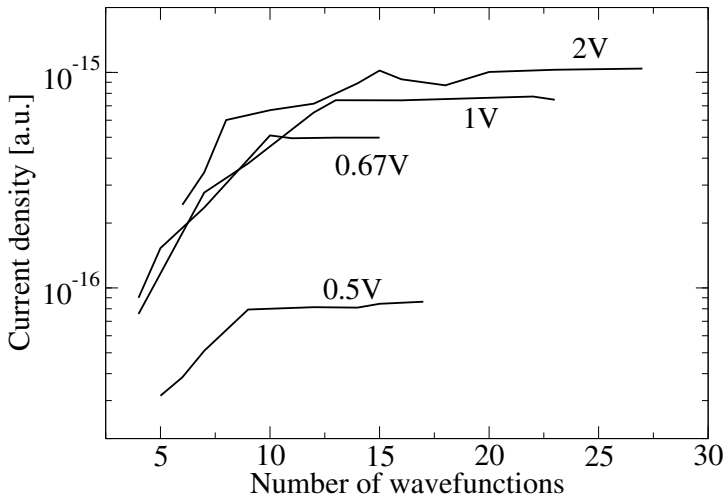

FIG. 2: Current density vs. number of wavefunctions for four different values of bias (i.e. 0.5, 0.67, 1, and 2V)

The energies and wavefunctions were calculated by solving the envelope function Schrödinger equation, within the effective mass approximation, implementing the finite difference solver. This approach intrinsically enforces the 'hard wall' boundary conditions, which in turn defines the continuum discretation.

We should note that the presented model is general and can be applied to any QW structure, with an arbitrary number of discrete states, and delivers a direct estimate of the physical observables, as well as input parameters used in other phenomenological simulations (capture probability, drift velocity). Moreover, the simulation is independent of the materials used, and can be employed for evaluation of QWIP characteristics, for materials where empirical estimates as well as experimental data are not available.

Next we present numerical results obtained from our model, for the usual GaAs/AlGaAs QWIP structure design for detection at $\sim 8.5\mu$m (see Ref. [16]), as well as a comparison with experimental data. The modelled QWIP consists of 40 periods, with well and barrier widths of 40 and 342 Å, respectively and an Al content in the barrier layer of 26.3%. The wells are assumed to be doped with an effective sheet carrier density of $1.8 \times 10^{11}\text{cm}^{-2}$ and the temperature was set to 77K. Electron -longitudinal optical (LO) phonon scattering was taken as the main scattering mechanism and calculated as in Ref. [17]. Electron-electron and impurity scattering was considered to be negligible as continuum states are hardly populated and the doping density is low.

The a priori task was to verify the first assumption of our model, that the continuum can be, for this purpose, accurately presented by a finite set of discrete wavefunctions. In order to prove that, we have calculated the current density as a function of the number of wavefunctions used in our

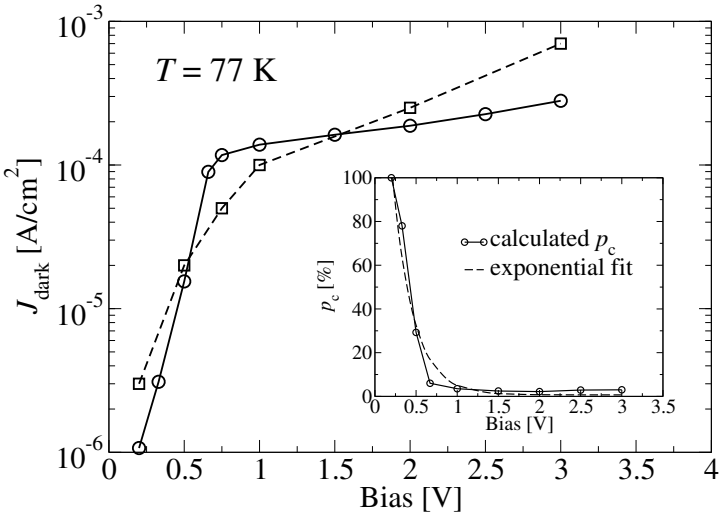

FIG. 3: Calculated (solid line and circles) and experimental (dashed line and squares) dark current density/voltage characteristics at 77 K. Inset: Calculated capture probability vs. bias (circles) and the appropriate exponential fit (dashed line).

basis for a few values of the external bias (Fig. 2). It can be seen that the current density converges with an increasing number of states. It is expected that the necessary number of wavefunctions increases with the increase of the bias, as the energy range between the two ground states of the adjacent periods increases. It is interesing to note that the convergence corresponds to an average spacing between adjacent continuum states of a few meV.

The next step was to compare the calculated dark current density with experimental results. In Fig. 3 both the calculated and the experimental current/voltage characteristics are presented. A good agreement is achieved for the whole range of examined voltages with an average discrepancy of a factor of two. This may be partly due to leakage on contacts, or due to scattering mechanisms not taken into account in the simulation, and is within expectation. In the inset of Fig. 3 the calculated capture probability is given as a function of the applied bias. It exhibits steep decay at lower biases (from 0.3 to 0.5V) and saturation at higher voltages ($>$ 1V). The simulated dependence generally follows the exponential decay (usually assumed in the literature; see Ref.[16] and [18]), except in the mid-range of voltages between, 0.5 and 1V, where the exponential dependence overestimates the capture probability.

Fig. 4 shows the responsivity as a function of the applied voltage for detection at 8.5μm. The absorption linewidth was assumed to be 50meV for the bound-continuum transition ($\Delta\lambda/\lambda \sim$ 33%). The responsivity curve exhibits nonlinear behavior at lower biases, reaching a peak value of around 0.3A/W. Furthermore, a decrease at higher biases is observed, which is the consequence of the absorption line shifting to higher wavelengths with an increase of the applied bias. As the

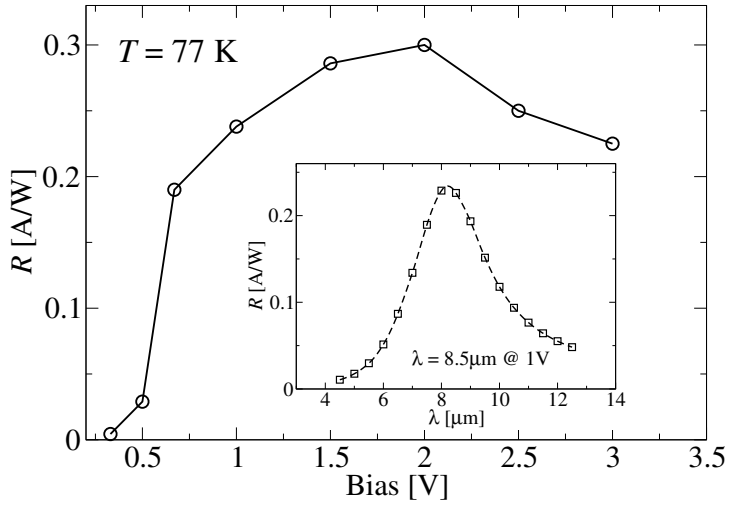

FIG. 4: Calculated responsivity vs. applied bias at 77K for the fixed wavelength of 8.5μm. Inset: wavelength dependence of the responsivity for 1V bias

experimental data for the calculated QWIP structure do not exist we have compared our results with available data for a fairly similar structure (see Fig.10 in Ref. [16]) and again found good agreement, as well as with both the high and low bias behaviour. The wavelength dependence of the responsivity at 1V bias is given in the inset. The responsivity approximately follows the Lorentzian shape profile as expected, with peak at $\sim 8.5\mu$m.

In conclusion we presented a detailed, fully microscopic model for electron transport in QWIPs. The model is based on fully self-consistent rate equations approach within the 'tight-binding' approximation, applied by including the interaction with two nearest neighbors. Macroscopic parameters like current density, responsivity and capture probability are obtainable without need for empirical parameters. In order to examine the accuracy of the simulation we have applied it to a GaAs/AlGaAs QWIP, and found very good agreement with the experiment for dark current, capture probability, as well as both the bias and spectral dependence of the responsivity. The presented model can be applied to any QWIP device, and can be very useful for examining novel structures and materials.

The authors would like to acknowledge discussions with Richard Soref. V. D. J. would like to thank the School of Electronic and Electrical Engineering for funding.

[1] A. Rogalski, J. Appl. Phys. **93**, 4355 (2003).

[2] L. Jiang, S. S. Li, M. Z. Tidrow, W. R. Dyer, W. K. Liu, J. M. Fastenau, T. R. Yurasits, Appl. Phys. Lett.**79**, 2982 (2001).

[3] M. Z. Tidrow, X. Jiang, S. S. Li, K. Bacher, Appl. Phys. Lett. **74**, 1335 (1999).

[4] H. C. Liu, R. Dudek, A. Shen, E. Dupont, C. Y. Song, Z. R. Wasilewski, M. Buchanan, Appl. Phys. Lett. **79**, 4237 (2001).

[5] V. Ryzhii, M. Ryzhii, H. C. Liu, J. Appl. Phys. **92**, 207 (2002).

[6] M. Ryzhii, V. Ryzhii, M. Willander, J. Appl. Phys. **84**, 3403 (1998).

[7] J. L. Pan, C. G. Fonstad, IEEE J. Quant. Electron. **35**, 1673 (1999).

[8] M. Ershov, H. C. Liu, J. Appl. Phys. **86**, 6580 (1999).

[9] S. D. Gunapala, S. V. Bandara, J. K. Liu, E. M. Luong, N. Stetson, C. A. Shott, J. J. Bock, S. B. Rafol, J. M. Mumolo, M. J. McKelvey, IEEE Trans. Electron. Dev. **47**, 326 (2000).

[10] S. D. Gunapala, S. V. Bandara, A. Singh, J. K. Liu, S. B. Rafol, E. M. Luong, J. M. Mumolo, N. Q. Tran, D. Z.-Y. Ting, J. D. Vincent, C. A. Shott, J. Long, P. D. LeVan, IEEE Trans. Electron. Dev. **47**, 963 (2000).

[11] N. E. I. Etteh, P. Harrison, J. Appl. Phys. **92**, 248 (2002).

[12] M. A. Gadir, P. Harrison, R. A. Soref, Appl. Phys. Lett. **81**, 4272 (2002).

[13] O. O. Cellek, C. Besikci, Semicond. Sci. Technol. **19**, 183 (2004).

[14] D. Indjin, P. Harrison, R. W. Kelsall, Z. Ikonić, Appl. Phys. Lett. **82**, 1347 (2003).

[15] V. Jovanović, D. Indjin, Z. Ikonić, V. Milanović, J. Radovanović, Solid State Commun. **121**, 619 (2002).

[16] L. Thibaudeau, P. Bois, J. Y. Duboz, J. Appl. Phys. **79**, 446 (1996).

[17] P. Harrison, *Quantum Wells, Wires and Dots: Theoretical and Computational Physics* (John Wiley & Sons Ltd, Chichester,1999)

[18] B. F. Levine, J. Appl. Phys. **74**, R1 (1993).